Influence of substrate topography on the growth and magnetic properties of obliquely deposited amorphous nanocolumns of Fe–Ni

2009 J. Phys. D: Appl. Phys. 42 215005

(http://iopscience.iop.org/0022-3727/42/21/215005)

IOP PUBLISHING JOURNAL OF PHYSICS D: APPLIED PHYSICS

J. Phys. D: Appl. Phys. **42** (2009) 215005 (8pp) doi:10.1088/0022-3727/42/21/215005

Influence of substrate topography on the growth and magnetic properties of obliquely deposited amorphous nanocolumns of Fe–Ni

Senoy Thomas[1], S H Al-Harthi[2], I A Al-Omari[2], R V Ramanujan[3], V Swaminathan[3] and M R Anantharaman[1,4]

[1] Department of Physics, Cochin University of Science and Technology, Cochin 682022, India
[2] Department of Physics, College of Science, Sultan Qaboos University, PO Box 36, Postal Code 123, Muscat, Sultanate of Oman
[3] School of Materials Science and Engineering, Nanyang Avenue, Nanyang Technological University, Singapore 639798, Singapore

E-mail: senoythomas@yahoo.co.in and mraiyer@gmail.com

Received 11 May 2009, in final form 30 August 2009
Published 13 October 2009
Online at stacks.iop.org/JPhysD/42/215005

Abstract

We investigated the influence of substrate surface roughness on the structural and magnetic properties of obliquely deposited amorphous nanocolumns of Fe–Ni. Experiments showed that the surface roughness of the substrate greatly determines the morphology of the columnar structures and this in turn has a profound influence on the magnetic properties. Nucleation of Fe–Ni nanocolumns on a smooth silicon substrate was at random, while that on a rough glass substrate was defined by the irregularities on the substrate surface. It has been found that magnetic interaction between the nanocolumns prepared on a silicon substrate was due to their small inter-column separation. Well separated nanocolumns on a glass substrate resulted in exchange isolated magnetic domains. The size, shape and the distribution of nanocolumns can be tailored by appropriately choosing the surface roughness of the substrate. This will find potential applications in thin film magnetism.

(Some figures in this article are in colour only in the electronic version)

1. Introduction

Soft magnetic materials based on Fe–Ni are of considerable interest due to their potential applications in magnetic sensors and magnetic recording heads [1–10]. With the advent of this material exhibiting excellent soft magnetic properties, the nanostructured form of this has found use in miniaturized magnetic devices. Several strategies have been developed for the growth of nanostructured magnetic materials [11–15]. Nanolithography-based methods, solution-based approaches and template-based methods are some of them. Some of these methods, however, require high temperatures and special conditions while in other cases, they demand complex and tedious procedures. For instance, in template assisted growth of nanostructures, the selection of suitable catalysts and templates is not straightforward, and the removal of templates and the stabilization of unsupported nanostructures represent crucial issues that may compromise the structural and physical properties. The capability of obtaining ordered arrays of well-defined and periodic nanostructures in an accurate, fast and inexpensive fashion would be of considerable interest not only from an applied perspective but also from a fundamental point of view.

Oblique angle vapour deposition offers advantages associated with fabrication of nanostructures over large areas, as required in many advanced technological and industrial applications [16–23]. In this technique, vapour deposition is carried out on to a substrate oriented at an oblique angle to

[4] Author to whom any correspondence should be addressed.

the vapour source. The vapour atoms travel to the substrate at oblique angles relative to the surface normal of the substrate. The evaporant nucleates on the substrate; the region behind the nucleus does not receive any further vapour because of the shadowing by the nucleus. Therefore, vapour will be deposited only onto the nucleus. This preferential growth dynamics gives rise to the formation of isolated columnar structures. Some advantages of this technique are the non-requirement of templates, relatively low temperatures and less harmful chemicals for the nanostructure fabrication [24].

Generally, the morphology of the nanostructures thus obtained is influenced by the substrate surface roughness and the growth conditions used for the film formation along with oblique angle, deposition rate, deposition time, etc. The growth of nanostructures will be the resultant of the competition between the smoothening due to adatom surface diffusion and roughening by self-shadowing. For the synthesis of well-defined nanostructures having appropriate separation and clear surface morphologies, an understanding on the interplay between the mechanisms involved in the growth process is essential. From an applied standpoint, a detailed knowledge of the growth behaviour of the nanostructures on a solid surface will aid in synthesizing nanostructures with well-defined roughness and geometry.

To date, ferromagnetic nanocolumns have been grown by vapour phase co-deposition and oblique angle vapour deposition [25–28]. Fe–Ni–Co nanocolumns were grown by the self-organization of vapour phase co-deposited Fe–Ni–Co [26]. Nanocolumns with Co/Cu bilayers were obtained by two-source oblique angle vapour deposition [27]. Recently, we studied the surface evolution of amorphous nanocolumns of Fe–Ni obtained by oblique angle vapour deposition on a silicon substrate [29]. It was found that the growth of nanostructures on a silicon substrate was more or less random and surface diffusion of adatoms led to the coarsening of the columns at higher deposition time. There are many potentially attractive applications for these columnar films, if they can be prepared with the desired microstructure and inter-column separation within the practical limits of time and expense. A critical issue concerning the achievement of this goal is the control of nucleation. The nucleation events occur preferentially on defects and abnormalities on a substrate surface. While so much work has been devoted to understanding the effect of deposition parameters on the morphology of elementary metal nanocolumns [30–33], there have been fewer efforts to understand the influence of substrate topography on the growth mechanisms and magnetic properties of nanostructures of amorphous alloys. A study relating the substrate surface roughness to column evolution and magnetic properties will be important not only from a fundamental perspective but also from an applied standpoint. The main objective of this work is to investigate the influence of substrate surface roughness on the morphology and the separation between the nanostructures in oblique angle vapour deposition. Fe–Ni based amorphous nanocolumnar structures were obtained on silicon and glass substrates having different initial surface features. Commercially available Metglas 2826 MB ribbon of composition $Fe_{40}Ni_{38}Mo_4B_{18}$ was employed as a source material to deposit Fe–Ni columnar thin films. Growth of columns on different substrates is studied using atomic force microscopy (AFM). Further, the evolution of magnetic properties with column growth is studied using AFM and magnetic force microscopy (MFM) techniques. The combined use of AFM and MFM will aid in understanding the intricate relationship between the magnetic properties and the nanoscale sized surface features. The MFM measurements are supplemented with vibrating sample magnetometry (VSM) to correlate the average magnetic properties with microstructure.

2. Experiment

2.1. Preparation

Commercially available Metglas 2826 MB ribbon of composition $Fe_{40}Ni_{38}Mo_4B_{18}$ was employed as a source material to deposit Fe–Ni thin films on silicon (coded as sample A) and glass substrates (coded as sample B). The substrates were cleaned with acetone, ethanol and trichloroethylene and were immediately loaded into the vacuum chamber. The substrate was tilted in such a way that the angle between the surface normal to the substrate and the direction of incoming flux was at an oblique angle of 40°. No substrate rotation was provided. The films were deposited by thermal evaporation using a current of 25 A at a base pressure of 1×10^{-5} mbar onto substrates oriented at an oblique angle of 40° to the flux. The base pressure of $\sim 1 \times 10^{-5}$ mbar was achieved by a diffusion pump backed with a rotary pump. The source to substrate distance was 26 cm. A set of samples were also grown on sodium chloride substrates for transmission electron microscopy (TEM) investigations.

2.2. Characterization

TEM experiments were carried out in a Jeol JEM-2200 FS electron microscope operated at 200 kV. The compositions of the films were analysed using an energy dispersive x-ray spectrometer which was attached to the TEM column. X-ray photoelectron spectroscopy (XPS) measurements were carried out using an Omicron Nanotechnology Multiprobe Instrument. XPS spectra were obtained using a high resolution hemisphere analyzer EA 125 HR equipped with a detection system consisting of seven channeltrons. A monochromated Al Kα source of energy $h\nu = 1486.6$ eV was used to probe the films which was attached to a molybdenum sample holder. Pressure in the XPS chamber during the measurements was 5×10^{-10} mbar. The imaging of magnetic domains was performed with a commercial AFM (Veeco Instrument, Multimode) operated in tapping plus lift mode. This ensures separation between the topographic and magnetic data. A commercial Si tip coated with a CoCr thin film (80 nm thick) that was magnetized vertically was used (Micro Masch NSC35/Co–Cr). The radius of curvature of the tip was less than 90 nm. The full tip cone angle was less than 30°. Images were collected at different tip to sample separations (lift height) ranging from 30–120 nm. Room temperature magnetization measurements were carried out using a vibrating sample magnetometer (DMS 1660 VSM) with an external field varying

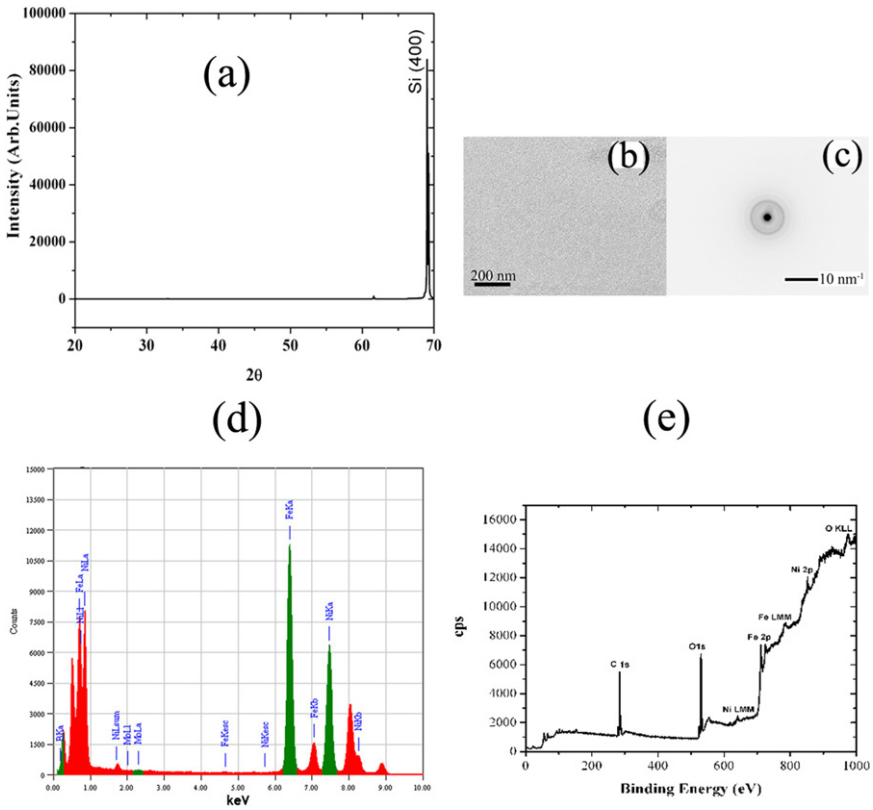

Figure 1. (*a*) XRD pattern for a film grown on a silicon substrate, (*b*) TEM bright field image of thin film, (*c*) corresponding electron diffraction pattern, (*d*) energy dispersive x-ray spectrum for the film and (*e*) XPS survey scan of the nanocolumns on a silicon substrate.

from −5 to +5 kOe. Cross sectional TEM measurements were carried out in a JEOL-2010 microscope operated at 200 keV.

3. Results and discussions

3.1. Structure and composition

The x-ray diffraction (XRD) patterns of the two samples were featureless except for the peaks from the substrates. Figure 1(*a*) shows the XRD of the film grown on the Si substrate. The diffraction pattern indicates that the prepared samples are amorphous in nature. TEM bright field image (plan view) of the sample is shown in figure 1(*b*). The microstructure exhibits contrasts typical of an amorphous material. The electron diffraction pattern (figure 1(*c*)) consists of a diffraction ring which is characteristic of an amorphous material.

Figure 1(*d*) depicts the energy dispersive x-ray spectrum obtained during TEM measurements. The spectrum shows the presence of Fe and Ni. The composition of the films was estimated from the peak intensities of Fe Kα and Ni Kα lines in the spectrum after background subtraction. The atomic percentage of Fe and Ni was 55 and 45, respectively. XPS survey scan was collected for films coated on Si substrates (figure 1(*e*)). The spectrum exhibits photoelectron lines characteristic of Fe, Ni, O and C. The C 1s peak corresponds to the contaminant carbon on the top surface of the specimen. The O 1s spectrum consists of peaks originating from oxygen in metal–oxygen bond. The survey scan also exhibited lines corresponding to the emission of Auger electrons (Ni LMM, Fe LMM and O KLL).

3.2. Evolution of morphology with substrate roughness

Characterization of the substrate surface was performed using an atomic force microscope. Figures 2(*a*) and (*b*) show 3D AFM images of silicon and glass substrates. The best known parameter characterizing the morphology of a surface is its root mean square (rms) roughness. The rms roughness obtained from the AFM images for silicon and glass substrates was 0.77 nm and 3.38 nm, respectively.

Figures 3(*a*) and (*b*) show the topographic images of films coated on silicon (coded as sample A) and glass substrates (coded as sample B), respectively. A clear difference in morphology of the films obtained on the two different substrates was observed. The lateral size of the columns on a silicon substrate is small (∼250 nm) as well as they are closely packed (average separation between the columns ∼240 nm), while well separated (average separation between the columns ∼570 nm) and larger columns were obtained on a glass substrate (lateral size around 450 nm). The measured rms roughness was ∼3.16 nm and 8.64 nm for sample sets A and B, respectively. In both cases the rms roughness was smaller than the total film thickness (∼50 nm), which suggests that there are film deposits in between the columns. The line scans shown in figure 4 illustrate the size of the nanocolumns on both silicon and glass substrates. Tip convolution effects result in an exaggerated column width and in an actual case the width of the column could be much less [34].

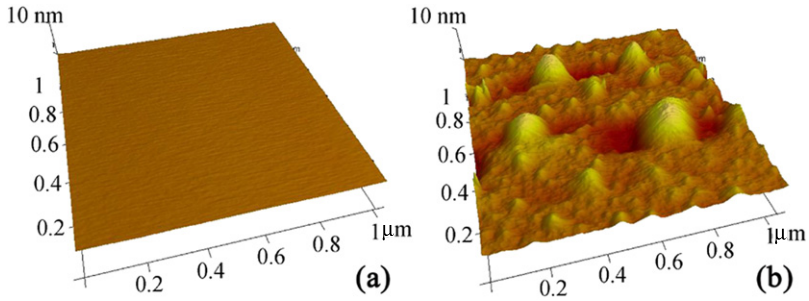

Figure 2. 3D AFM image of (*a*) Si surface (*b*) glass surface.

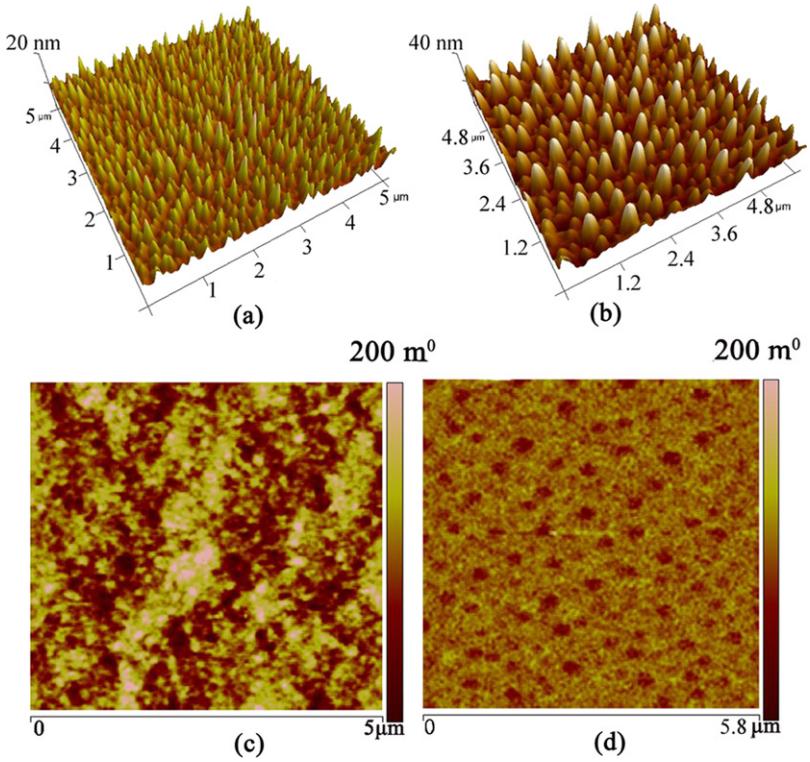

Figure 3. 3D AFM images for columns on (*a*) Si substrate (*b*) on glass substrate. MFM images for columns on (*c*) Si substrate (*d*) on glass substrate. Lift height in MFM scans is 60 nm.

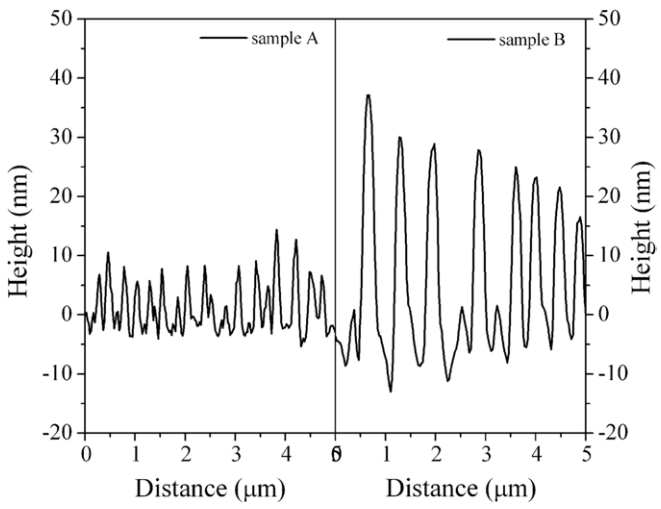

Figure 4. Line scans along the surface of samples A and B.

Columnar growth is a result of atomic shadowing mechanisms that occur at the substrate surface [16]. During the initial stages of vapour deposition, adatoms condense onto the substrate and form individual separated islands or nuclei. When the substrate is tilted such that the incident vapour arrives at oblique angles, the topography of adatom nuclei results in geometrical shadowing over regions of the substrate, preventing the coalescence of nuclei into a continuous thin film layer. The nuclei capture the vapour flux that would have landed in the shadowed regions, resulting in the formation of columns.

Deposition on smooth substrates generally results in a pseudo-random arrangement of nucleation sites during the initial stages of film growth, producing a similar distribution of columns over the substrate surface [20]. On the other hand, if there is a small perturbation to a flat surface, the irregularities act as nucleation sites for the columnar structure [30]. The topographical variations define the shadow regions on the substrate during the initial stages of film growth so that adatom

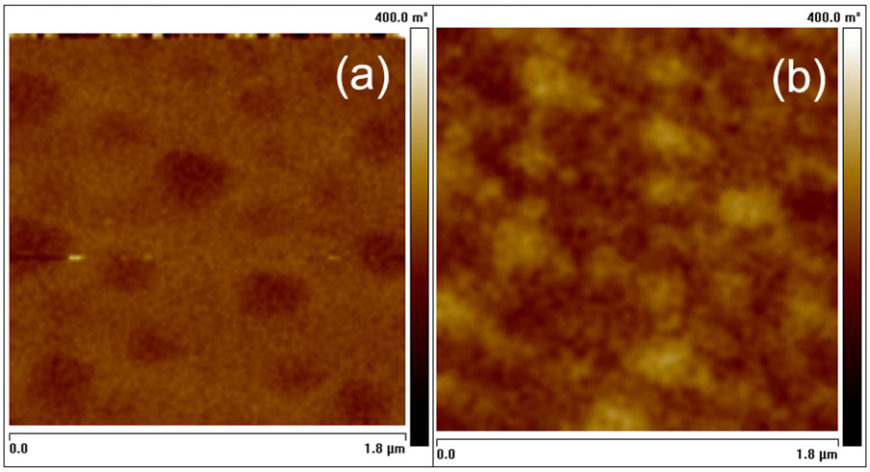

Figure 5. (1.8 × 1.8) μm^2 MFM images of sample B obtained at a lift height of 100 nm under two different tip magnetization orientations (z scale is 400 m°).

nucleation is forced to occur on the surface protrusions. The small perturbations on the flat surface increase with time because surface protrusions receive more flux than valleys. If the protrusions are high enough, their shadows extend to its neighbour and suppress the inter-seed film growth. This can be a reason for the decreased inter-columnar competition in a sample prepared on a glass substrate, where the initial irregularities were 2–3 nm in height. In glass substrates the column evolution is defined by the topographic protrusions on its surface, while in silicon it is defined by the Fe–Ni clusters formed initially. In films deposited on glass substrates, the separation between the columns was defined by the position of the irregularities on the substrate surface. Random nucleation on a smooth silicon surface resulted in randomly arranged nanocolumns.

3.3. Magnetic properties

3.3.1. MFM studies. MFM with a cantilever vibrating normal to the sample is sensitive to the gradient of the tip–sample interaction force in the normal direction of vibration, that is to $\partial F_Z/\partial Z$ [35, 36]. The interaction force is $F = m \cdot \nabla H$, where m is the tip moment and H is the field at the tip. When the tip is ideally hard (e.g. coated with CoCr) and of constant moment m_z directed normal to the sample surface, the MFM signal is proportional to $m_z(\partial^2 H_z/\partial Z^2)$, that is it is sensitive to the second derivative of the normal component of the sample field. The contrast in the MFM image is thus proportional to the gradient of the magnetic force between the tip and the sample. Figure 3(*c*) is an MFM image of sample A obtained at a lift height (tip–sample separation) of 60 nm. The contrast seen in the MFM images implies the presence of magnetic domains with out-of plane magnetic component. Sizes of the domains are larger than the width of individual columns which means that in this film there exists a magnetic interaction between the individual columns. In figure 3(*d*) an MFM image of sample B indicates the existence of well separated circular domains. The microstructure of this film is that of well separated larger columns and the MFM image from the corresponding scan area reveals that the out-of plane magnetic component is only from individual columns. A one-to-one correspondence can be seen between the columns in the AFM image and circular domains in the MFM image of sample B (figures 3(*b*) and (*d*)). It is seen from the AFM images that the lateral size of columns for the two sample sets A and B is, correspondingly, 250 nm and 450 nm. While MFM images showed that the magnetic domain size is around 1.5 μm and 450 nm for the sample sets A and B, respectively. This gives a clear indication that in sample A, magnetic correlation length is beyond the lateral size of individual columns. Thus in sample A the magnetic structure is determined not only by the individual columns but also by the magnetic interactions between them. The magnetic correlation length in sample B is within the column width itself, which means that the columns in sample B are exchange isolated.

In order to ensure that the contrast in the MFM image of sample B is caused by the film magnetization and not due to topographical artefacts, the tip magnetization was reversed by 180° and an MFM scan was obtained from the same area. Because it was not possible to relocate the scanning probe exactly on the same scan line after removal of the tip for remagnetization, exact mirror symmetry between the traces could not be expected. Figure 5(*b*) shows the MFM image of sample B for a lift height of 100 nm obtained after reversing the tip magnetization. The phase shift is now positive and the contrast shifted from dark to bright (when compared with MFM image in figure 5(*a*)) which is an indication of the fact that the contributions to the MFM images are a result of magnetic forces of the sample.

Figure 6 shows the topography and corresponding MFM images of sample B for a lift height of 30, 60 and 100 nm. The plot of phase shift versus lift height (figure 7) showed an exponential decay, in agreement with our expectations. This decay in phase shift with lift height is due to the decay with distance of magnetic force from the sample.

3.3.2. VSM studies. In order to gather more insight on the magnetic behaviour of the columns, room temperature magnetization measurements were performed on the two

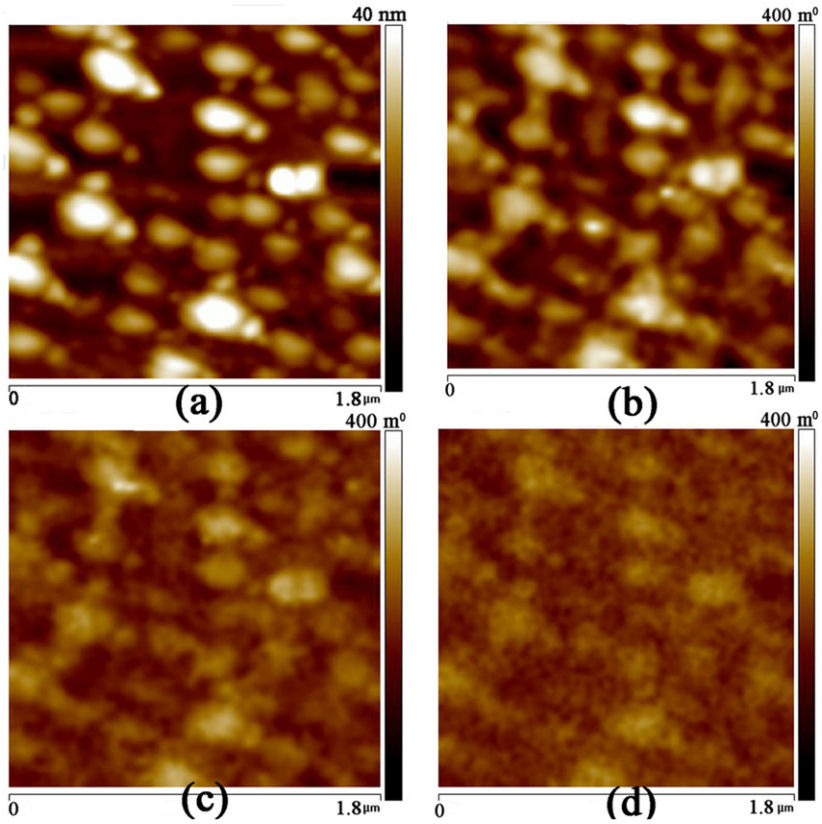

Figure 6. (*a*) Topography. (*b*) Phase image at lift height of 30 nm (*c*) 60 nm and (*d*) 100 nm for sample B.

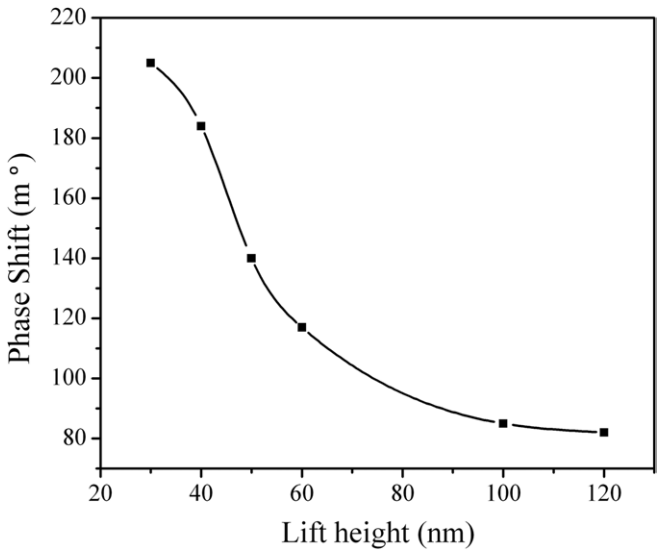

Figure 7. Scanning height dependence of phase shift in sample B.

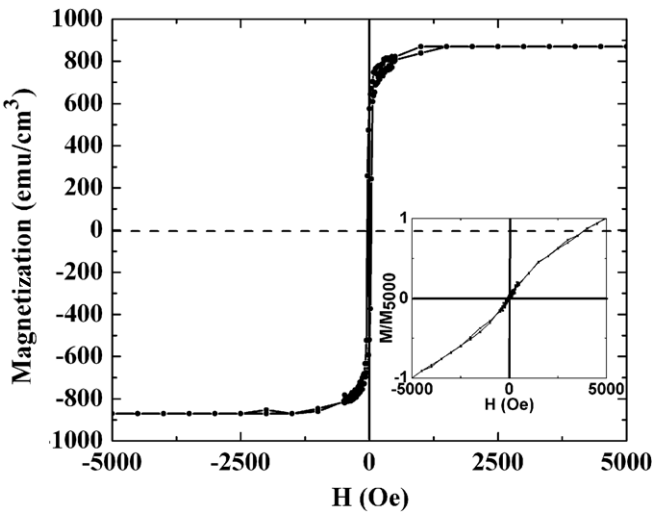

Figure 8. Room temperature hysteresis loop for nanocolumns on Si substrate in parallel field. Inset shows the loop recorded in a perpendicular field.

sample sets using a vibrating sample magnetometer. The measurements were carried out both in parallel (in-plane) and perpendicular fields (out-of-plane). Figures 8 and 9 show the magnetization curves for sample sets A and B, respectively. The saturation magnetization was found to be ∼870 emu cm^{-3} in both cases. It is to be noted that a low field was only necessary to saturate the magnetization in the in-plane direction while a field as high as 5000 Oe could not saturate the material in the out-of-plane direction. AFM studies showed that the film roughness is smaller than the total film thickness, implying that there are film deposits in between the columns. In any columnar growth the trade-off is between the adatom surface diffusion and self-shadowing. Such a growth on a randomly seeded substrate usually results in deposits in between the columns. Because of these deposits, the portion close to the substrate will become a continuous layer and the geometry of the whole system will be layer plus island type,

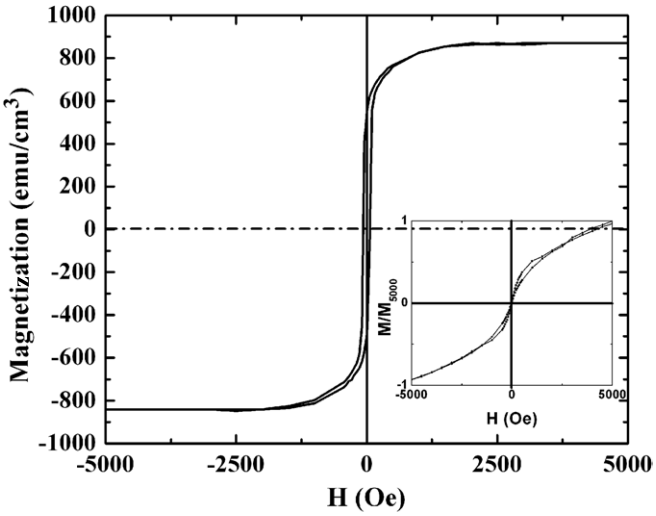

Figure 9. Room temperature hysteresis loop for nanocolumns on glass substrate in parallel field. Inset shows the loop recorded in a perpendicular field.

in which islands are arranged on top of the layer. This is further supported by the cross sectional TEM image shown in figure 10. The presence of Fe–Ni islands on the top of Fe–Ni layer is clear from figure 10. The height of the islands is found to be around 20 nm and the film thickness is around 50 nm. Due to the absence of significant magnetocrystalline anisotropy, the magnetization direction will be largely influenced by the shape anisotropy. Within the layer, since the long axis is along the substrate plane, the magnetic direction will be in plane. On the other hand, in the islands, where the long axis is perpendicular to the substrate plane, the magnetic direction will be out of plane. The magnetization measurements using VSM will have contributions from the whole sample and one will only note signatures of in-plane magnetic direction because of the domination of the contributions emanating from the layer. However, MFM being sensitive to the surface, detects the out-of-plane component from the islands. The measurements show that the perpendicular magnetic component from the columns is small due to their small aspect ratio. The in-plane hysteresis loops show that the field necessary to saturate sample B (∼2000 Oe) is double that required for sample A (∼1000 Oe). This can be correlated with the morphology of the columns prepared in two conditions (figure 11).

In sample A the columns are packed close together (average inter-column distance around 240 nm) and MFM showed that there is a magnetic interaction between the columns. On the other hand, in sample B, the columns are well separated (average inter-column distance around 570 nm) and magnetic interaction between the columns is minimal. Besides domain wall motion, domain rotation is required for saturating the specimen in the in-plane direction. Since the islands of sample B are non-interacting, a larger magnetic field is required for the complete rotation of moments in the island, towards the field direction. This field required for sample A will be less due to the magnetic interaction existing in between the islands. Another feature to be noted from the in-plane hysteresis loop (figures 8 and 9) is that coercivity of sample B (∼65 Oe) is larger than that of sample A (∼40 Oe). This can be due to the

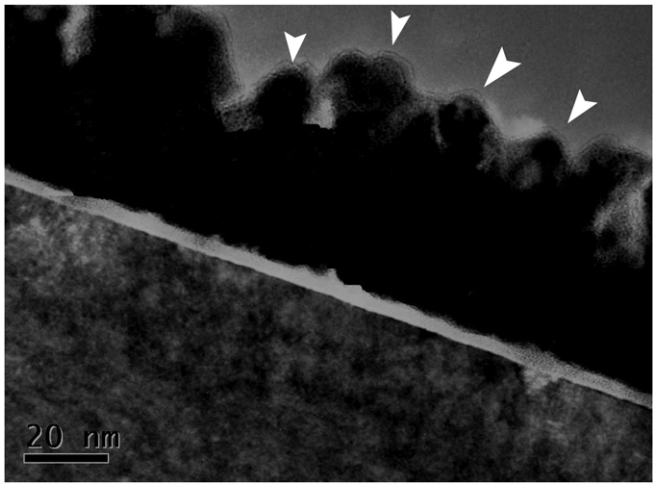

Figure 10. Cross sectional TEM of Fe–Ni films on a silicon substrate (the arrows show the position of islands).

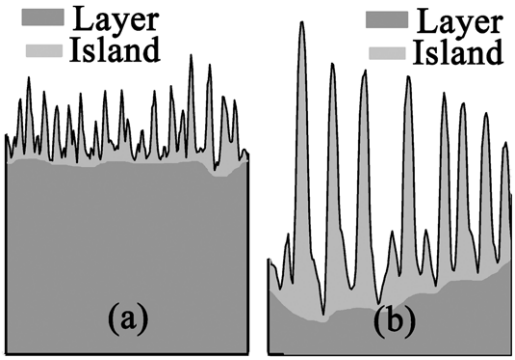

Figure 11. Schematic of the film structure in (*a*) sample A and (*b*) sample B.

increased surface roughness of sample B. Small irregularities on the surface of a film inhibit the passage of a domain wall because the energy stored within a domain wall surrounding such a region is smaller than in an undisturbed domain wall and consequently the system energy must be increased to enable the domain wall motion. This is consistent with our previous observations in swift heavy ion irradiated Fe–Ni thin films [37].

4. Conclusions

Magnetic columnar thin films based on Fe–Ni were obtained by oblique angle deposition. Initial surface roughness of the substrate played a decisive role in the final morphology of the columnar structures. Thicker and taller columns were obtained on a glass substrate when compared with that on a smoother silicon substrate. Nucleation of Fe–Ni nanocolumns on a smooth silicon substrate was at random, while that on a rough glass substrate was defined by the irregularities on the substrate surface. The morphology of the resultant films determined their magnetic properties. Due to their small inter-column separation, magnetic interaction was present for nanocolumn arrays prepared on silicon substrates. On the other hand, well separated nanocolumns on a glass substrate resulted in exchange isolated magnetic domains. These results

also indicate that oblique angle deposition on a patterned substrate can result in well separated nanocolumns which can be promising for future high density recording applications.

Acknowledgments

This work is supported by the Inter University Accelerator Centre New Delhi, India, through UGC Funded University Project, UFUP No 35306. Senoy Thomas acknowledges CSIR, New Delhi, for the senior research fellowship. RVR acknowledges the support of SERC, Singapore, grant No 0621010032. Al-Omari would like to thank Sultan Qaboos University for the support under grant number IG-SCI-PHYS-07-05. Al-Harthi would like to thank Sultan Qaboos University for the support under the grant number IG-SCI-PHYS-09-04. The authors acknowledge IIT Bombay for extending scanning electron microscopy facility under the Indian Nanoelectronics Users Programme.

References

[1] Hasegawa R 2004 *Mater. Sci. Eng.* A **375** 90
[2] McHenry M E, Willard M A and David E 1999 *Prog. Mater. Sci.* **44** 291
[3] Wang S X, Sun N X, Yamaguchi M and Yabukami S 2000 *Nature* **407** 150
[4] Hernando A, Vazquez M and Barandiaran J M 1988 *J. Phys. E: Sci. Instrum.* **21** 1129
[5] Osaka T, Takai M, Hayashi K, Ohashi K, Saito M and Yamada K 1998 *Nature* **392** 796
[6] Hayakawa Y, Makino A, Fujimori H and Inoue A 1997 *J. Appl. Phys.* **81** 3747
[7] Vazquez M and Hernando A 1996 *J. Phys. D: Appl. Phys* **29** 939
[8] Thomas S, Al-Harthi S H, Sakthikumar D, Al-Omari I A, Ramanujan R V, Yasuhiko Yoshida and Anantharaman M R 2008 *J. Phys. D: Appl. Phys.* **41** 155009
[9] Komova E, Varga M, Varga R, Vojtanik P, Bednarcik J, Kovac J, Provencio M and Vazquez M 2008 *Appl. Phys. Lett.* **93** 062502
[10] Du S W and Ramanujan R V 2005 *J. Non-Cryst. Solids* **351** 3105
[11] Liu X, Fu L, Hong S, Dravid V P and Mirkin C A 2002 *Adv. Mater.* **14** 231
[12] Sun S, Zeng H, Robinson D B, Raoux S, Rice P M, Wang S X and Li G 2004 *J. Am. Chem. Soc.* **126** 273
[13] Sun S, Murray C B, Weller D, Folks L and Moser A 2000 *Science* **287** 1989
[14] Hyeon T 2003 *Chem. Commun.* **8** 927
[15] Azzaroni O, Schilardi P L and Salvarezza R C 2002 *Appl. Phys. Lett.* **80** 1061
[16] Hawkeye M M and Brett M J 2007 *J. Vac. Sci. Technol.* A **25** 1317
[17] Robbie K and Brett M J 1997 *J. Vac. Sci. Technol.* A **15** 1460
[18] Dick B, Brett M J, Smy T J, Freeman M R, Malac M and Egerton R F 2000 *J. Vac. Sci. Technol.* A **18** 1838
[19] Messier R and Lakhatiah A 1999 *Mater. Res. Innov.* **2** 217
[20] Steele J J and Brett M J 2007 *J. Mater. Sci. Mater. Electron.* **18** 367
[21] Jensen M O and Brett M J 2005 *IEEE Trans. Nanotechnol.* **4** 269
[22] Zhao Y-P, Ye D-X, Wang G-C and Lu T-M 2003 *Nanotubes and Nanowires* vol 5219 ed A Lakhtakia and S Maksimenko (Bellingham, WA: SPIE Optical Engineering Press) p 59 (*Proc. SPIE*)
[23] Demirel M C, Boduroglu S, Cetinkaya M and Lakhtakia A 2007 *Langmuir* **23** 5861
[24] Tang X-J, Zhang G and Zhao Y-P 2006 *Nanotechnology* **17** 4439
[25] Lisfi A, Lodder J C, Wormeester H and Poelsema B 2002 *Phys. Rev.* B **66** 174420
[26] Greve H, Biswas A, Schürmann U, Zaporojtchenko V and Faupel F 2006 *Appl. Phys. Lett.* **88** 123103
[27] Kar A K, Morrow P, Tang X-T, Parker T C, Li H, Dai J-Y, Shima M and Wang G C 2007 *Nanotechnology* **18** 295702
[28] Carl A, Kirsch S, Lohau J, Weinforth H and Wassermann E F 1999 *IEEE Trans. Magn.* **35** 3106
[29] Thomas S, Al-Harthi S H, Ramanujan R V, Bangchuan Z, Yan L, Lan W and Anantharaman M R 2009 *Appl. Phys. Lett.* **94** 063110
[30] Bai P, McDonald J F, Lu T-M and Costa M J 1991 *J. Vac. Sci. Technol.* A **9** 2113
[31] Rechendorff K, Hovgaard M B, Chevallier J, Foss M and Besenbacher F 2005 *Appl. Phys. Lett.* **87** 073105
[32] Dolatshahi-Pirouz M B, Hovgaard M B, Rechendorff K, Chevallier J, Foss M and Besenbacher F 2008 *Phys. Rev.* B **77** 115427
[33] Alouach H and Mankey G J 2005 *Appl. Phys. Lett.* **86** 123114
[34] Rasa M, Kuipers B W M and Philipse A P 2002 *J. Colloid Interface Sci.* **250** 303
[35] Porthun S, Abelmann L and Lodder C 1998 *J. Magn. Magn. Mater.* **182** 238
[36] Hartmann U 1999 *Annu. Rev. Mater. Sci.* **29** 53
[37] Thomas S, Thomas H, Avasthi D K, Tripathi A, Ramanujan R V and Anantharaman M R 2009 *J. Appl. Phys.* **105** 033910